J. Fluid Mech. (1998), *vol.* 356, *pp.* 199–220. Printed in the United Kingdom

A numerical investigation of steady convection in mushy layers during the directional solidification of binary alloys

By T. P. SCHULZE† AND M. GRAE WORSTER

Department of Applied Mathematics and Theoretical Physics, University of Cambridge, Silver Street, Cambridge CB3 9EW, UK

(Received 15 October 1996 and in revised form 12 September 1997)

We present a numerical study of steady convection in a two-dimensional mushy layer during the directional solidification of a binary mixture. The calculations reveal the internal structure of strongly nonlinear states featuring upflow which has been focused into solid-free regions known as chimneys. The mushy layer is modelled as a porous medium whose permeability is a function of the local solid fraction. The mushy layer is coupled to a chimney that is modelled as a narrow vertical channel where lubrication scalings are used to simplify the Navier–Stokes equations. We use these methods to exhibit solutions which give the detailed structure of the temperature, solute, flow and solid-fraction fields within the mushy layer. A key finding of the numerics is that there are two distinct chimney solutions at low Rayleigh numbers, presumably corresponding to stable and unstable portions of a subcritical solution branch. We also explore the relationship between convective solutions with and without chimneys.

1. Introduction

Interfacial instability during the solidification of binary mixtures (Mullins & Sekerka 1964) frequently leads to the formation of a layer of dendrites at the solid/liquid interface. These 'mushy' layers are common in both industrial and geophysical settings, and have been the focus of many recent investigations. General reviews of mushy layers and the convective processes that take place within them are given by Worster (1992*a*, 1997).

Our focus here is on steadily convecting solutions within the mushy layer once the flow has been focused into discrete solid-free regions that puncture the mushy layer at roughly periodic intervals. These defects in the mushy layer are known as 'chimneys', and they can occur when an alloy is cooled from below and rejects some or all of the lighter component of the mixture, or when it is cooled from above and rejects the heavier of the two components. The rise (or fall) of the rejected material due to solutal buoyancy results in a decreased freezing temperature, which may be sufficient to inhibit solidification locally. When this occurs, upflow (downflow) is enhanced by the increased permeability, and becomes focused in narrow, solid-free vertical channels. Experiments using aqueous solutions of ammonium chloride (Copley *et al.* 1970; Tait & Jaupart 1992; Chen 1995) provide a convenient means of viewing chimneys in the laboratory (figure 1). Chimneys have also been studied

† Present address: Courant Institute, New York University, 251 Mercer St., New York, NY 10012, USA.

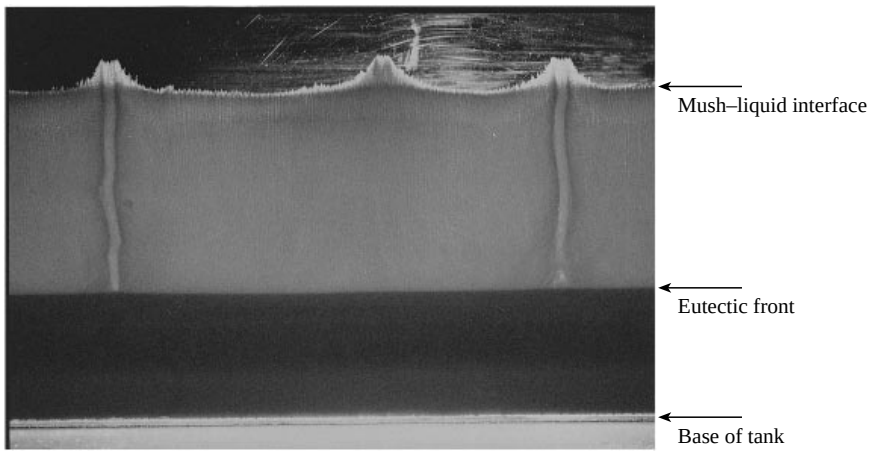

FIGURE 1. A photograph of mushy layer chimneys during an experiment with an ammonium-chloride solution. In this system, pure ammonium-chloride crystals are formed when the solution is cooled below its freezing temperature, leaving behind a diluted solution with a density lower than that of the bulk fluid. In the present case, the mushy layer is growing away from a fixed cold base which is at a temperature below the eutectic point, so that both the solid–mush and mush–liquid interfaces are advancing at a decreasing rate. At the time the photograph was taken the distance between the base of the tank and the eutectic front was approximately 3 cm. Notice that the chimney walls and the mush–liquid interface are flat to a good first approximation.

in experiments using metallic alloys (Sarazin & Hellawell 1988; Hellawell, Sarazin & Steube 1993), NaCl–water solutions (Wettlaufer, Worster & Huppert 1997) and alcohol–water solutions (Worster 1997).

Interest in the chimney phenomenon stems from two sources. In industrial settings, chimneys are responsible for the formation of 'freckles' in cast binary alloys. Freckles result when the chimney solidifies, leaving behind narrow cylindrical regions within the solid which have a composition and microstructure differing significantly from the bulk of the material. Such non-uniformities are highly undesirable and much of the research on mushy layers has been motivated by a desire to understand and prevent the formation of freckles. A knowledge of the solute fluxes through chimneys is also needed in order to determine the bulk composition of solidified materials. In geophysical settings, chimneys are known to form within sea ice in polar oceans (Eide & Martin 1975) and are believed to form within magma chambers (Tait & Jaupart 1992) and the Earth's inner core (Fearn, Loper & Roberts 1981). A better understanding of the fluxes from chimneys will help to determine the driving force for the abyssal circulation of the oceans and the geodynamo.

The theoretical investigation of convection in mushy layers has a history which goes back nearly thirty years. A thermodynamically consistent model of a mushy layer treated as an additional phase of matter was proposed by Hills, Loper & Roberts (1983), who developed equations governing the evolution of the mass-averaged properties of the layer. Alternative derivations of similar equations governing the volume-averaged properties have since been given by Fowler (1985) and Worster (1992*a*). These equations have been subjected to linear stability analyses (Fowler 1985; Worster 1992*b*; Chen, Lu & Yang 1994) and, more recently, weakly nonlinear analyses (Amberg & Homsy 1993; Anderson & Worster 1995). In the linear and weakly nonlinear analysis, there is no chimney *per se* – just a region of reduced solid fraction at the upflowing centres of convection cells.

Emms (1993) has performed numerical computations which follow the evolution of the solid fraction in the mushy layer until it becomes negative, at which point the model breaks down; the region of negative solid fraction needs to be replaced by a pure liquid region. Emms's computations are based on a model put forward by Emms & Fowler (1994) which assumes a mushy layer of fixed permeability and approximates the convection in the liquid region as a nearly uniform downflow.

The studies featuring fully developed chimneys fall into two groups. Roberts & Loper (1983) were the first to consider flow through a fully developed chimney, modelled as a cylindrical tube of uniform cross-section surrounded by an annular mushy layer of fixed permeability. This study was built upon by Worster (1991), who coupled the permeablility to the local solid fraction and deduced a scaling for the thermal boundary layer surrounding the chimney. The approach of these authors jumps past the development of the chimney by assuming a computational domain with the same physical characteristics seen in the laboratory. No numerical solutions for this model have been presented to date. All of the remaining mushy layer studies that feature anything resembling a chimney (for example, Bennon & Incropera 1987; Felicelli, Heinrich & Poirier 1991; Neilson & Incropera 1991, 1993) have been based on the Darcy–Brinkman equation, which models both the liquid and mushy regions by using a hybrid of the Navier–Stokes and Darcy equations. An advantage of this approach is that it eliminates the need to track the location of the mush–liquid interface. A disadvantage is that it normally requires one to resolve the mushy layer on the same scale as the chimney. To date, all of the solutions using this method have been poorly resolved.

The present study adopts the first of these two approaches. Motivated by experimental photographs, such as that shown in figure 1, we model the boundaries of our convection cell as being flat. We present detailed numerical solutions for a two-dimensional mushy layer punctured by chimneys at periodic intervals. While the same physical mechanisms are responsible for the formation of chimneys in planar and axisymmetric geometries, there are subtle differences in the way various quantities scale, and care should be taken when comparing our study with axisymmetric studies. In practice, most experimentally observed chimneys are approximately axisymmetric, but there have been some experiments on chimneys formed in Hele-Shaw cells (Chen 1995; Solomon & Hartley 1998) which come close to approximating the two-dimensional geometry considered here.

We present the governing equations and boundary conditions in §2. In §3, we outline the boundary-layer structure which emerges for large Rayleigh numbers, using the scaling analysis to motivate some of the boundary conditions used in the subsequent numerical analysis. The numerical procedures are briefly described in §4. In §5, we use these methods to exhibit solutions which give the detailed structure of the temperature, solute, flow and solid-fraction fields within the mushy layer. This simple model also provides insight into a possible distinction between strongly nonlinear convective solutions with and without chimneys. Our calculations in §6 are aimed at accounting for the portion of the mush–liquid boundary where it rises sharply to meet the cold fluid emerging from the chimney. We summarize our results in §7.

2. Formulation

Consider the physical domain consisting of a horizontal mushy layer sandwiched between semi-infinite liquid and solid layers. A steady state with this geometry can be established by forcing liquid at constant speed through a temperature gradient

that is fixed in the laboratory frame of reference. In practice the liquid must be confined in some way – in a Hele-Shaw cell, for example. The processing of material in this manner is commonly referred to as directional solidification. Note, however, that this directional solidification at constant speed differs from the case where material is solidified by cooling from a fixed boundary. While the latter case is more representative of geophysical applications and has been the focus of the previous numerical studies, it is less desirable for theoretical purposes because the solid–liquid and mush–liquid interfaces slow down as time advances, and the system is always in a transient state. Both cases are common in industrial applications.

We seek steady solutions for a half-cell of a periodically extended system. To this end, the mushy layer is further divided into two domains, corresponding to zero-solid-fraction chimneys and finite-solid-fraction mushy regions. The two domains are separated by a boundary (the chimney wall) where the the solid fraction is approximately zero. In principle, one can formulate a free boundary problem where the chimney wall is, for example, the locus of points where the solid fraction approaches zero continuously. This is a very challenging problem which remains to be solved. In practice, chimneys have nearly vertical sidewalls and appear to extend to the bottom of the mushy layer (see figure 1). Hence, we shall constrain the chimney wall to be flat and vertical but allow its width to adjust dynamically to the flow by requiring the solid fraction to be zero at mid-height on the chimney wall. We demonstrate that this leads to solutions where the solid fraction is close to zero along the entire wall when the mass flux through the chimney becomes large.

With the aim of keeping our model as simple as possible, we ignore thermal buoyancy and solutal diffusion, which are normally small effects. We also assume that the mush–liquid interface advances slowly, so that the mushy layer remains in local thermodynamic equilibrium, and take the solid and liquid to have the same densisty, so that phase-change convection is ignored. Finally, we assume that all of the lighter component of the mixture is rejected upon solidification and that the liquidus relationship is linear, conditions which are approximately true in many systems, including ammonium-chloride–water.

Using this idealized model, one can scale the temperature and concentration so that, within the mushy region, they are equal to one another:

$$\theta = [T - T_L(C_0)]\,/\Delta T = (C - C_0)/\Delta C. \tag{2.1}$$

Here $\Delta T = \Gamma\,\Delta C = T_L(C_0) - T_E$ is the difference between the liquidus temperature at the far-field concentration and the eutectic temperature, $\Delta C = C_0 - C_E$ is the difference between the far-field concentration and the eutectic concentration and Γ is the slope of the liquidus.

Following the formulation of Worster (1991), we treat the mushy region as a porous medium, in which the flow is governed by Darcy's equation with variable permeability Π:

$$\boldsymbol{u} = -Ra\Pi\left(\nabla p + \theta\hat{\boldsymbol{k}}\right). \tag{2.2}$$

We have non-dimensionalized this equation by scaling the Darcy velocity (volume flux of fluid per unit area) $\boldsymbol{u}$ with the vertical pulling speed (solidification rate) V, distance with the thermal diffusion length scale κ/V, permeability with a characteristic value Π_0 and pressure with $\beta\Delta C\rho_0 g\kappa/V$, where β is the solutal expansion coefficient, g is the acceleration due to gravity and ρ_0 is a reference density.

An important feature of mushy layer dynamics is that the permeability varies with the solid fraction. Despite this, many studies have either assumed a fixed permeability or avoided the issue by choosing scalings that make this effect weak. Here, we assume that the permeability Π depends on the local solid fraction ϕ as

$$\Pi = (1-\phi)^3. \tag{2.3}$$

Amberg & Homsy (1993) explore the influence of varying the exponent in this power law within their asymptotic model. Note that, with this law, the permeability drops to zero as the solid fraction approaches unity, but remains finite as the solid fraction approaches zero.

The governing equations in the bulk of the mushy region are given by conservation of heat and solute, along with (2.2), which we recast in terms of a streamfunction ψ:

$$\nabla^2\theta + \theta_z = \boldsymbol{u}\cdot\nabla\theta + S\phi_z, \tag{2.4a}$$

$$\theta_z + \mathscr{C}\phi_z = \boldsymbol{u}\cdot\nabla\theta + (\phi\theta)_z, \tag{2.4b}$$

$$\nabla^2\psi = -Ra\,\Pi\,\theta_x + (\nabla\Pi\cdot\nabla\psi)/\Pi. \tag{2.4c}$$

Here the stream function is defined by $\boldsymbol{u} = \nabla\times(\psi\hat{\boldsymbol{j}})$, where $\hat{\boldsymbol{j}}$ is a unit vector orthogonal to the plane of the two-dimensional mushy layer and oriented out of the plane of our x, z coordinate system. The non-dimensional variables in these equations are the Stefan number S, a concentration ratio $\mathscr{C}$ and the solutal porous-medium Rayleigh number Ra:

$$S = \frac{\mathscr{L}}{c\Delta T}, \quad \mathscr{C} = \frac{C_S - C_0}{\Delta C}, \quad Ra = \frac{\beta\Delta C g \Pi_0}{\nu V}, \tag{2.5a–c}$$

where $\mathscr{L}$ is the latent heat of fusion, c is the specific heat, C_S is the concentration of the solid forming the dendrites and ν is the kinematic viscosity.

Within the chimney and the liquid region above the mushy layer, the solid fraction is zero and the temperature and concentration are unconstrained by the liquidus relationship. The non-dimensional governing equations are conservation of heat, solute and mass, along with the Navier–Stokes equations:

$$\nabla^2 T + T_z = \boldsymbol{u}\cdot\nabla T, \tag{2.6a}$$

$$C_z = \boldsymbol{u}\cdot\nabla C, \tag{2.6b}$$

$$\nabla\cdot\boldsymbol{u} = 0, \tag{2.6c}$$

$$\nabla^2\boldsymbol{u} = (1/Pr)(\boldsymbol{u}\cdot\nabla\boldsymbol{u} - \boldsymbol{u}_z) + (Ra/Da)(C\hat{\boldsymbol{k}} + \nabla p), \tag{2.6d}$$

where the new non-dimensional parameters are the Prandtl and Darcy numbers:

$$Pr = \frac{\nu}{\kappa}, \quad Da = \frac{\Pi_0 V^2}{\kappa^2}. \tag{2.7a,b}$$

The Darcy number is the ratio of the permeability scale to the thermal-diffusion length scale, and must be small for the porous-medium assumption to hold.

Avoiding the solution of equations (2.6) in the liquid region above the mushy layer is one of the principal simplifications sought in this study. In order to accomplish this, one must make assumptions about the values of the pressure, temperature and temperature gradient along the top of the mushy layer. Following the example of previous authors (see, for example, Fowler 1985; Amberg & Homsy 1993 or Emms & Fowler 1994), we assume that the top of the mushy layer has both constant temperature and constant dynamic pressure. The latter can be derived formally in the limit of small Darcy number (Emms & Fowler 1994). More difficult is the condition

on the temperature gradient, which, in principle, can be used to determine the shape of the mush–liquid boundary. This boundary condition is discussed in some detail in the following section, where we ultimately decide to determine the location of the top of the mushy layer in an approximate manner by considering a heat balance across the interface at the centre point which divides two chimney catchment regions.

A complete set of boundary conditions for equations (2.4*a–c*) is given by constant temperature and continuity of mass flux at the lower boundary; constant temperature, constant pressure and zero solid fraction at the top; continuity of pressure and continuity of heat flux at the chimney wall; and symmetry conditions at the centreline dividing two chimney catchment regions:

$$\theta = -1, \quad \psi = 0 \quad \text{at} \quad z = 0, \tag{2.8a}$$

$$\theta = \phi = p = 0 \quad \text{at} \quad z = h, \tag{2.8b}$$

$$p|_c^m = \hat{\boldsymbol{n}} \cdot \nabla\theta|_c^m = 0 \quad \text{at} \quad x = a, \tag{2.8c}$$

$$\theta_x = \psi = 0 \quad \text{at} \quad x = L, \tag{2.8d}$$

where jump conditions are indicated with the m (mushy region) and c (chimney region) super/subscripts, L is half the non-dimensional chimney spacing, a is the half-width of the chimney, h is the height of the layer and $\hat{\boldsymbol{n}}$ is a unit vector normal to the interface. The two elliptic equations (2.4*a, c*) require information on each of the boundaries for both the flow and thermal fields. Equation (2.4*b*) requires information on the solid fraction to be supplied along the top boundary; this information is then propogated downward by the vertical motion of the crystal. These nine boundary conditions are sufficient to close the system, provided we know the location of the free boundaries. For the purposes of the numerical portion of this study, these boundaries will be determined in an approximate manner, using the conditions alluded to previously.

The boundary conditions in the chimney region consist of continuity of temperature, pressure and mass flux at the top of the chimney; constant temperature, constant concentration, continuity of mass flux and the no-slip condition at the base of the chimney; symmetry conditions at the centre of the chimney; and continuity of temperature, concentration and mass flux, along with the no-slip condition at the chimney wall:

$$T = C = -1, \quad \psi = \psi_z = 0 \quad \text{at} \quad z = 0, \tag{2.9a}$$

$$\psi = \psi_{xx} = T_x = 0 \quad \text{at} \quad x = 0, \tag{2.9b}$$

$$T|_c^m = C|_c^m = \psi|_c^m = \boldsymbol{u} \cdot \hat{\boldsymbol{t}} = 0 \quad \text{at} \quad x = a, \tag{2.9c}$$

where $\hat{\boldsymbol{t}}$ is a unit vector tangent to the interface. Boundary conditions at the top of the chimney are not used in our analysis, owing to the use of a lubrication approximation in this region.

3. Scaling analysis

The scaling analysis put forward in this section serves two purposes. Firstly, it provides a framework within which the subsequent numerical analysis can be interpreted by revealing the dominant mechanisms which govern distinct regions of the mushy layer. Secondly, it suggests approximate boundary conditions that can be used to simplify the numerical analysis and it reveals the significance of the errors made in applying these approximations. We emphasize, however, that the numerics in the remainder of this paper rely only on the lubrication approximation within the

chimney and are not dependent on the more specific distinguished limit considered here. As is often the case, the asymptotic and numerical approaches complement one another – the former offering insight into the large-Rayleigh-number behaviour of the system while the latter is better suited to $O(1)$-Rayleigh-number computations.

Given the large number of parameters in the system, there are several distinguished limits which one might consider. Our efforts here are guided by the ammonium-chloride–water system, a key attribute of that system being its relatively low solid fraction. We choose a distinguished limit which preserves this feature as the Rayleigh number becomes large:

$$Ra \sim \mathscr{C} \gg 1. \tag{3.1}$$

In this limit one finds that the mass flux through the mushy layer grows with the Rayleigh number. Alternative scalings that have an $O(1)$ mass flux and an asymptotically vanishing permeability for large Rayleigh numbers can also be found. The Darcy number must be small for the porous-medium assumption to hold; further, we shall assume

$$Ra^{4/9} Da^{1/3} \ll 1, \tag{3.2}$$

so that the thermal field within the chimney is horizontally uniform to leading order (see (3.8) below). Assuming a Darcy number of $O(10^{-5})$ and a Rayleigh number of $O(10)$, the quantity on the left of (3.2) is about 6×10^{-2}. We assume the remaining parameters to be $O(1)$.

The regime we consider is similar to the large-Rayleigh-number limit in Bénard convection (Turcotte 1967; Roberts 1979; Emms & Fowler 1994) in that there is a large, inertially dominated central core in the liquid region which is isothermal and, in the present case, has a uniform concentration as well (see figure 2). In the case of Bénard convection between two parallel boundaries, diffusive boundary layers are formed at the upper and lower boundaries and along the regions joining convection cells. In the present case the upper boundary is taken to be at infinity, with the result that temperature and concentration in the core region take on the far-field values. The lower boundary layer includes the mushy layer itself, which indicates that the height of the mushy layer shrinks with increasing Rayleigh number, provided the far-field temperature remains fixed. Note that this new understanding corrects the tacit assumption in the scaling analysis of Worster (1991) that the vertical scale of the mushy layer is independent of the Rayleigh number. A consequence of this is the conclusion that there is no region of the mushy layer in which the isotherms are horizontal to leading order at large Rayleigh number.

Looking to the mushy layer, the considerations just mentioned imply that the dominant balance in equation (2.4*a*) is between vertical diffusion and advection. In equation (2.4*b*) we consider the distinguished limit where the advective terms are balanced by the source term for solute released upon solidification, and in equation (2.4*c*) we maintain the balance between the viscosity and buoyancy:

$$\theta_{zz} \sim \boldsymbol{u} \cdot \nabla \theta, \tag{3.3a}$$

$$\mathscr{C} \phi_z \sim \boldsymbol{u} \cdot \nabla \theta, \tag{3.3b}$$

$$\psi_{zz} \sim -Ra \Pi\, \theta_x + \Pi_z \psi_z / \Pi. \tag{3.3c}$$

These balances imply the scalings

$$\psi \sim Ra^{1/3}, \quad h \sim Ra^{-1/3}, \quad \phi \sim Ra^{1/3} \mathscr{C}^{-1}, \quad \theta \sim 1. \tag{3.4a–d}$$

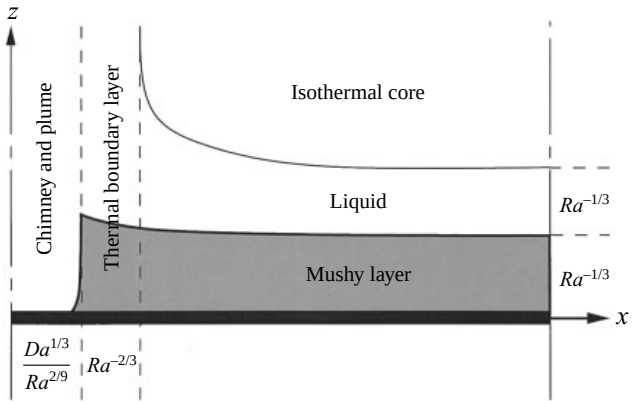

FIGURE 2. A diagram of the boundary layer structure in the mush–chimney system for the limit $Ra \gg 1$, $Da \ll 1$ and $\mathscr{C} \sim Ra$. In this limit the mass flux is large and the solid fraction is small. The chimney and thermal boundary layer scale like $Da^{1/3}/Ra^{2/9}$ and $Ra^{-2/3}$, respectively. The height of the mushy layer, and the thickness of the boundary layer in the liquid above the mushy layer both scale like $Ra^{-1/3}$.

Equations (3.3*a–c*) apply throughout most of the mushy layer, but a separate scaling must be found to allow for horizontal diffusion in a small region near the chimney. We refer to this region as the thermal boundary layer (see figure 2), and it is analogous to the thermal boundary layer suggested by the scaling analysis of Worster (1991). Physically it represents the effect of heat being drawn out of the mushy region as a result of cold fluid from the bottom of the layer moving up the chimney. The dominant balances within the boundary layer are given by

$$\theta_{xx} \sim \boldsymbol{u}\cdot\nabla\theta, \tag{3.5a}$$

$$\mathscr{C}\phi_z \sim \boldsymbol{u}\cdot\nabla\theta, \tag{3.5b}$$

$$\psi_{xx} \sim -Ra\Pi\,\theta_x + \Pi_x\psi_x/\Pi, \tag{3.5c}$$

where we have assumed that the stream function and the height of the mushy layer scale the same as in the outer region, implying that the bulk of the streamlines pass through both regions. From the balances in equations (3.5), the boundary layer thickness is found to be $O(Ra^{-2/3})$. Comparing equations (3.3*b*) and (3.5*b*) we see that $\phi \sim Ra/\mathscr{C} \sim 1$ in the thermal boundary layer. In the ammonium-chloride–water system, the concentration ratio is fairly large ($\mathscr{C} \approx 20$), and it is this fact that is responsible for the relatively low solid fraction in that system. So the combined limits of large concentration ratio and large Rayleigh number are consistent with our assumption of a highly permeable, high-mass-flux mushy layer.

Experimental observation reveals that chimneys are quite slender in practice, with a height that is many times their nearly uniform width. Taking advantage of this narrow geometry, the non-dimensional half-width of the chimney a is assumed to be small. Combining this assumption with the large-Rayleigh-number and small-Darcy-number assumptions, we consider the limit where the leading-order behaviour of the chimney is governed by

$$T_{xx} \sim 0, \tag{3.6a}$$

$$\boldsymbol{u}\cdot\nabla C \sim 0, \tag{3.6b}$$

$$\psi_{xxx} \sim \frac{Ra}{Da}(p_z + C), \tag{3.6c}$$

$$p_x \sim 0. \tag{3.6d}$$

Here, the stream function, temperature and height of the chimney are scaled as in (3.4*a–d*). We also have

$$a \sim \frac{Da^{1/3}}{Ra^{2/9}}, \quad p \sim Ra^{-1/3}. \tag{3.7a,b}$$

Thus, to leading order, the chimney has a diffusion-dominated thermal field, an advection-dominated concentration field and a flow field governed by lubrication theory. Unlike equations (3.3) and (3.5), equations (3.6) apply equally well for moderate as well as large Rayleigh numbers, owing to the narrow aspect ratio of the chimney and the smallness of the Darcy number.

Notice that equation (3.6*a*) implies that, to leading order, the temperature in the chimney is a function of z determined by the temperature at the chimney wall. This does not allow for the conduction of heat across the chimney wall, which is an important effect in the real system. As cold fluid rises up the chimney, it draws heat from out of the mushy region, resulting in an increased solid fraction in the area surrounding the chimney. This effect can be captured by including the leading-order correction to (3.6*a*), which accounts for the vertical advection of heat in the chimney:

$$T_{xx} = Da^{1/3} Ra^{4/9} \psi_x T_z, \tag{3.8}$$

where $Da^{1/3} Ra^{4/9} \ll 1$.

Integrating this equation and converting to coordinates scaled for the mushy region leads to an explicit boundary condition for the heat flux through the chimney wall:

$$T_x = \psi T_z \quad \text{at} \quad x = a. \tag{3.9}$$

This condition makes use of and replaces the jump condition requiring temperature gradients to match across the chimney wall, decoupling the thermal field in the mushy layer from that in the chimney at leading order.

We can gain some qualitative information on the actual shape of the chimney wall by applying the condition $\phi = 0$ along the entire boundary. This is equivalent to

$$\phi_z + \phi_x a_z = 0 \quad \text{at} \quad x = a(z), \tag{3.10}$$

which may be combined with the solute conservation equation (2.4*b*) to give

$$a_z = \frac{\boldsymbol{u} \cdot \nabla \theta - \theta_z}{\phi_x (\theta - \mathscr{C})}. \tag{3.11}$$

At the base of the mush–chimney boundary we have $w = \theta_x = 0$ and $\theta = -1$, so that this reduces to

$$a_z = \frac{\theta_z}{\phi_x (1 + \mathscr{C})}. \tag{3.12}$$

It is evident that θ increases away from the solid boundary and that ϕ increases as one moves into the mushy layer. We can therefore deduce that $a_z > 0$ at $x = z = 0$, indicating that chimneys narrow towards the bottom. By maintaining a flat vertical boundary in spite of this conclusion, we will find that there is a significant region of positive solid fraction near the base of our chimneys. The conclusion that chimneys narrow toward the bottom appears to apply specifically to the case where the solidification is taking place at constant speed. In contrast, experiments where the

dendrites are growing from a fixed cold boundary exhibit chimneys that flare out at the bottom.†

Moving to the top boundary, we find that the concentration is uniform throughout the liquid layer wherever the flow is downward, owing to the lack of solutal diffusion. Combining this information with the assumption that the temperature and concentration are coupled through the liquidus relationship gives us the condition that the top of the mushy layer is an isotherm:

$$T = C = \theta = 0 \quad \text{at} \quad z = h. \tag{3.13}$$

We note that the same boundary-layer thickness applies on the liquid side of the interface (see figure 2), so that the dominant balance is again given by equation (3.3*a*). Within this boundary layer, the continuity equation implies that the horizontal velocity is zero to leading order and the vertical component is a function of only the lateral coordinate. This allows equation (3.3*a*) to be integrated across the depth of the boundary layer, producing a relationship between the far-field temperature (which applies throughout the core of the liquid region) and the temperature gradient at the interface:

$$\theta_z = \theta_\infty(1 - \psi_x) \quad \text{at} \quad z = h, \tag{3.14}$$

where the non-dimensional temperature at infinity is defined by

$$\theta_\infty = (T_\infty - T_L(C_0))/\Delta T. \tag{3.15}$$

This condition, proposed by Fowler (1985), retains the effect of the vertical pulling speed which should be a small effect at large Rayleigh numbers, making it better suited to our calculations which are at moderate Rayleigh numbers. The condition breaks down near the chimney exit, owing to significant horizontal diffusion of heat. Unfortunately, there is no simple way of solving the equations within this region in order to relate the temperature gradient to the far-field temperature. We shall estimate the height of our flat-topped mushy layer model by applying (3.14) at the point where two chimney catchment regions meet the mush–liquid interface (i.e. $x = L$, $z = h$). Symmetry arguments suggest that the condition will be most accurate at this point.

4. Computational procedures

When we examine equations (3.3*a–c*) and (3.5*a–c*) we find that there is no essential simplification over the full governing equations (2.4*a–c*), and we choose to work with the latter in formulating a numerical approximation to the system. The asymptotic approximations in the chimney (equations (3.6*a–e*)), however, are significantly simplified versions of equations (2.6*a–d*), and we take full advantage of these approximations.

4.1. *Mushy region computations*

The equations in the mushy region (2.4) are solved iteratively using either direct inversion with a sparse solver or successive over relaxation (SOR) on the elliptic equations (2.4*a* and 2.4*c*) and a numerical integration of (2.4*b*) using the trapezoidal rule.

† D. E. Loper (private communication) has recently deduced that the chimneys formed in the case of continuous solidification at constant speed must pinch off just before reaching the bottom of the mushy layer. The essence of his argument hinges on the fact that material must be flowing into the solid at the fixed pulling speed. This downward flowing material is getting colder, but material which is flowing up into the chimney must be getting warmer if it is to rise above the liquidus.

With the understanding that the differential operators in the following equations are second-order-accurate central difference operators, the symbolic representation of the first half of the iteration for the direct inversion algorithm is

$$\nabla^2\theta^{(n)} + \theta_z^{(n)} = \boldsymbol{u}^{(n-1)} \cdot \nabla\theta^{(n-1)} + S\phi_z^{(n-1/2)}, \tag{4.1a}$$

$$\nabla^2\psi^{(n)} = -Ra\Pi^{(n-1/2)}\theta_x^{(n-1)} + (\nabla\Pi^{(n-1/2)} \cdot \nabla\psi^{(n-1)})/\Pi^{(n-1/2)}, \tag{4.1b}$$

where the superscripts indicate the value of a quantity at the nth iteration. At the end of each half iteration the values of θ and ψ on the boundary are updated, and the value of the solid fraction on the entire domain is determined by the direct integration of

$$\theta_z^{(n)} + \mathscr{C}\phi_z^{(n+1/2)} - (\theta^{(n)}\phi^{(n+1/2)})_z = \boldsymbol{u}^{(n)} \cdot \nabla\theta^{(n)}\mathrm{d}z. \tag{4.2}$$

For a fixed set of parameter values, one can trade the dependence on θ_∞ for dependence on the (assumed) constant height h. In this case, one need only invert the elliptic operators in (4.2) once during the entire iterative procedure, and the direct inversion method is much faster than the SOR algorithm, typically requiring between 100 and 1000 iterations and converging in less than a minute on an HP 715/50 workstation.

The same calculation using the SOR method typically requires ten times the number of iterations, with each iteration taking about the same amount of time. However, if one is going to do several calculations changing one or more parameters each time, one will want to keep θ_∞ fixed, allowing h to evolve iteratively to its equilibrium value. Using the direct inversion method requires reinverting the elliptic operators in (4.2) for each iteration, which slows the procedure down considerable, especially for small mesh sizes. In such cases it proves more efficient to use the SOR technique. When using SOR, the integration for the solid fraction is the same as in (4.2) and the elliptic equations are solved using the standard SOR algorithm (Press *et al.* 1992), with the nonlinear terms evaluated using data from the previous iteration.

4.2. *Chimney computations*

The asymptotic approximations introduced in §3 for the equations in the chimney region are valid for moderate as well as large values of the Rayleigh number, provided the Darcy number is sufficiently small. In practice, the Darcy number is roughly proportional to the square of the dendrite spacing, and is typically 10^{-3} or smaller.

The equations (3.6*a–d*) are dealt with in two ways. In one approach, they are solved by transforming them to a set of coupled ODEs and applying a fourth-order Runge–Kutta method, with shooting, to solve the resulting boundary value problem. In a second approach a quadratic Polhausen-type approximation is made for the concentration field, which then allows one to integrate the momentum equation exactly. We describe the shooting method first.

Examining equations (3.6*b*) one sees that the gradient of the concentration field is normal to the flow field, indicating that streamlines are also isopycnals. This suggests the use of streamline coordinates in the chimney. Replacing the (X, Z) coordinate system with a (Ψ, Z) system, equations (3.6*b–d*) reduce to

$$W(WW_\Psi)_\Psi = P_Z(Z) + C(\Psi) \quad \text{for} \quad 0 \leqslant \Psi \leqslant \Psi_w, \tag{4.3a}$$

$$W_\Psi = 0 \quad \text{at} \quad \Psi = 0, \tag{4.3b}$$

$$W = 0 \quad \text{at} \quad \Psi = \Psi_w, \tag{4.3c}$$

where $\Psi_w(Z)$ is the value of Ψ at the chimney wall and Z appears only as a parameter,

so that the pressure is determined from its value at the chimney wall. We have used capital letters to emphasize that these are the scaled equations, and that boundary data must be rescaled when matching to data in the mushy region.

A third boundary condition, which determines the location of the free boundary can be found by inverting the coordinate transformation:

$$X_\Psi = -1/W \quad \text{for} \quad 0 \leqslant \Psi \leqslant \Psi_w, \tag{4.4a}$$

$$X = A \quad \text{at} \quad \Psi = \Psi_w. \tag{4.4b}$$

Equation (4.4*a*) must be integrated in order to find the value of $\Psi_w(Z)$. The near-vertical chimney wall, combined with the no-slip condition, implies that W will be zero at $\Psi = \Psi_w$, creating a singular condition in equation (4.3*a*). To remedy this, we find the leading-order asymptotic solution in terms of $\Delta\Psi = \Psi - \Psi_w$:

$$W \sim c_0(Z)\Delta\Psi^{1/2}, \tag{4.5}$$

where $c_0(Z)$ is used as the shooting parameter. After choosing a value for c_0, (4.5) is applied at a fitting point close to the singularity, and the result is used to initialize a fourth-order Runge–Kutta routine which is then used to integrate (4.3*a*) to $\Psi = 0$. An improved guess for c_0 is made, and the procedure is repeated until (4.3*b*) is satisfied. When one has found the appropriate values of $c_0(Z)$ all along the chimney wall, equation (4.4) is integrated backward from $\Psi = 0$ until $X = A$, which determines the new value of Ψ_w. This entire procedure is coupled to the numerical scheme in the mushy region (§4.1) and is iterated until a steady state is reached.

Finally, we use a root-finding procedure in order to determine the approximate chimney width A that will result in the solid fraction being zero at mid-height on the chimney wall.

4.3. *Reduced chimney model*

The procedure outlined in the previous section is still numerically time-consuming. In order to reduce computation time further, so that a detailed exploration of the parameter space can be undertaken, we opt for a simpler process based on a Polhausen approximation similar to that used by Roberts & Loper (1983) and Worster (1991). The value of the streamfunction given by this method was compared to that given by the method described in the previous section, and it was found that the two methods agreed to within 10% or better along the entire chimney wall, with the greatest error occurring at the top of the chimney.

In the simplified model, we assume that the concentration profile in the chimney is given by a quadratic function in X with Z-dependent coefficients, which are determined by the value of C at the chimney wall along with the fact that the concentration is constant along streamlines:

$$C(A) = C_w, \quad C(0) = -1, \quad C_X(A) = 0. \tag{4.6a–c}$$

Here we have assumed that streamlines enter the chimney orthogonally to the nearly vertical chimney wall as a result of the no-slip condition on the liquid side of the interface. We also assume that the streamline flowing up the centre of the chimney carries material very close to the eutectic concentration. These conditions give the following approximation for C within the chimney:

$$C = -1 + 2\frac{C_w(Z)+1}{A}X - \frac{C_w(Z)+1}{A^2}X^2. \tag{4.7}$$

With the approximation (4.7) in hand, the momentum equation can be integrated exactly to give

$$\Psi = \frac{P_Z(Z)-1}{2}\left(\frac{X^3}{3}-A^2X\right)+\frac{1+C_w}{3A}\left(\frac{X^4}{4}-A^3X\right)-\frac{1+C_w}{12A^2}\left(\frac{X^5}{5}-A^4X\right). \tag{4.8}$$

Finally, (4.8) can be evaluated at the chimney wall and combined with (2.9) to give a new boundary condition on the mushy region:

$$\psi = \frac{Ra}{Da}\,a^3\left(\frac{\psi_x}{3RaH}+\frac{3}{20}(\theta+1)\right) \quad \text{at} \quad x=a. \tag{4.9}$$

Here we have used Darcy's equation (2.2) to eliminate the pressure term. Note that we have written this equation in terms of unscaled coordinates. In presenting our results, we find it useful to define the quantity $\mathscr{A} = \left(Ra/Da\right)^{1/3} a$ as a measure of the strength of the flow through a chimney. The boundary condition (4.9) can be applied directly to the mush, and removes the need for further consideration of the chimney region.

5. Discussion of computational results

In figure 3(*a–c*) we plot the scaled chimney width $\mathscr{A}$, the mushy layer height h and the volume flux circulating through the top of the mushy layer as functions of the Rayleigh number for the case $\mathscr{C} = 10$, $S = 1$, $\theta_\infty = 0.1$, $Da = 0.001$ and $L = 1.0$. These curves can be interpreted as portions of a bifurcation diagram. Our numerical results extend beyond the data shown in these graphs, but we choose not to present the data where the flow amplitude is small since our model with the flat chimney walls is aimed only at fully developed chimneys. We can, of course, be confident that there is a purely conductive state having no chimney ($a = 0$). In fact, comparing with the linear theory results of Worster (1991) reveals that our numerics reproduce the correct linear critical Rayleigh number when interfacial perturbations are neglected, but the inappropriateness of this model for the weak-convection regime is noticable from the fact the curves shown in figure 3(*a–c*) intersect the linear-critical point at a transcritical rather than pitchfork bifurcation (this asymmetry, noticeable only when the flow is weak, is introduced in applying condition (3.14) at only a single point on the top boundary). The linear critical point is shown in the figure for reference. Notice that the volume flux increases with increasing chimney width (decreasing mushy layer height) and that the bifurcation is subcritical. Below we speculate on the nature of the relationship of the chimney solutions to convective solutions without fully formed chimneys (like those corresponding to the linear and weakly nonlinear analysis).

One can gain a fairly general feel for how the curves in figure 3(*a–c*) deform as the parameter values are changed by tracking the location of the turning point Ra_{min}. In figure 4(*a–d*) we plot this information for a range of parameter values. The dotted curve in figure 4(*a*) gives the volume flux into the layer as a function of Rayleigh number for a fixed set of parameters, duplicating the plot in figure 3(*c*). Superimposed on this plot are three curves indicating the path of the turning point when each of the three parameters $\mathscr{C}$, θ_∞ and S is varied independently of the other two. In figure 4(*b–d*) we give a more quantitative description of the turning point location by plotting Ra_{min} as a function of $\mathscr{C}$, θ_∞ and S, with two of the three parameters fixed in each case.

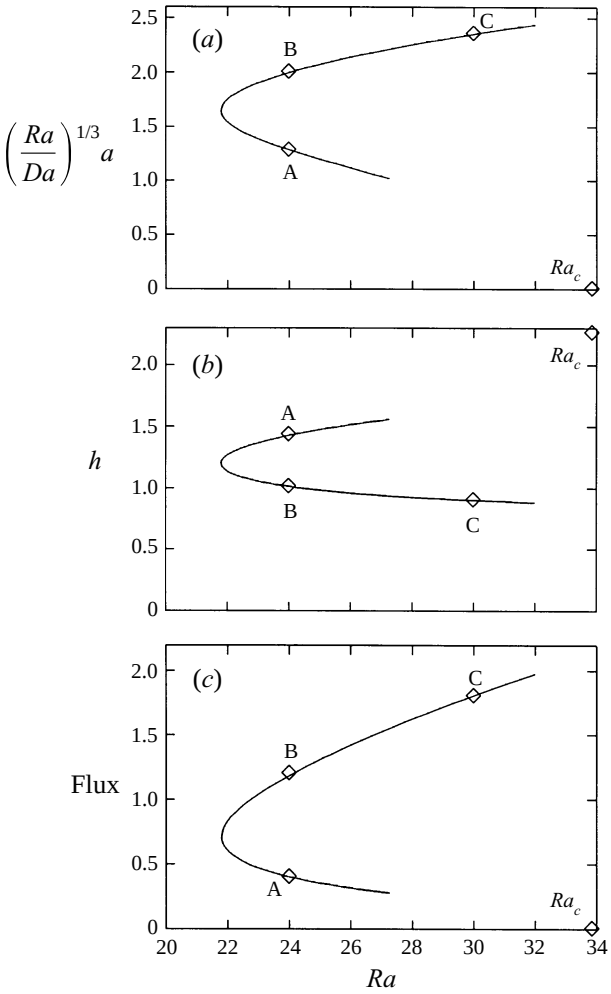

FIGURE 3. A plot of (*a*) scaled chimney width, (*b*) mushy layer height and (*c*) volume flux of fluid through the mushy layer as a function of Rayleigh number for $\mathscr{C} = 10$, $S = 1$, $\theta_\infty = 0.1$, $Da = 0.001$ and $L = 1.0$. For given values of a and Ra, the solid fraction (at mid-height) on the chimney wall is less than zero to the right of these curves. The details of the three points labelled A, B and C are shown in figure 5(*a–c*).

5.1. *Mushy layer structure*

The details of the solutions at the three points marked on figure 3(*a–c*) can be found in figure 5(*a–c*), where we plot streamlines in both the chimney and mushy regions, along with contours for temperature and solid fraction in the mushy region. The boundary condition requiring the pressure at the top of the mushy layer be constant combined with Darcy's equation (2.2) implies that the streamlines are vertical at the top of the layer. The streamlines may, however, leave the mushy layer through the chimney at oblique angles because the no-slip condition is applicable only on the liquid side of the mush–chimney interface. As a result, there is a discontinuity in the slope of the streamlines as they cross into the chimney.

The isotherms clearly show the existence of a thermal boundary layer that shrinks with increasing Rayleigh number. The boundary layer results from increasingly large

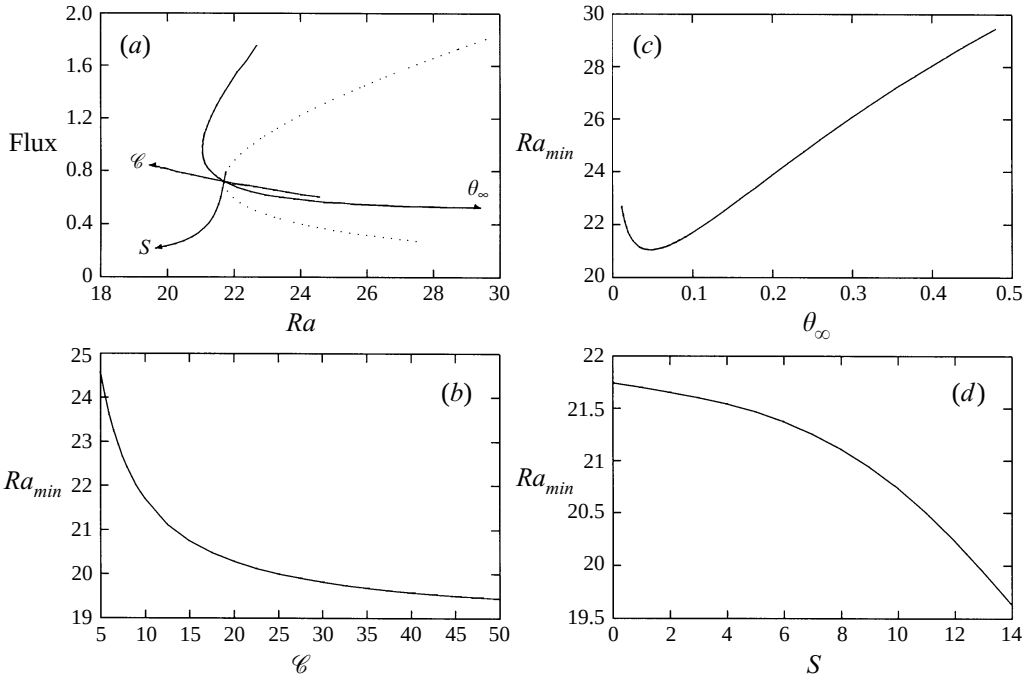

FIGURE 4. The dotted curve in (*a*) is a replot of figure 3(*c*), giving the volume flux into the layer as a function of Rayleigh number for a fixed set of parameters. Superimposed on this plot are three solid curves indicating the path of the turning point when each of the three parameters $\mathscr{C}$, θ_∞ and S is varied independently of the other two. Thus, all three of the turning point paths pass through the turning point of the dashed curve. The parameter ranges shown are $5 < \mathscr{C} < 50$, $0.01 < \theta_\infty < 0.5$ and $0 < S < 14$. The curves (*b–d*) show Ra_{min} as a function of these variables in the given ranges.

amounts of cold fluid being swept up the chimney as the strength of the flow increases. This has the secondary effect of increasing the solid fraction in the immediate neighbourhood of the chimney. Indeed, the isotherms near the top of the mushy layer have a shape which is reminiscent of the experimentally observed shape of the mush–liquid interface (see figure 1), despite the fact that the flat-top approximation is being used. The chimney itself is prevented from freezing because increasingly large amounts of solute are also being swept up the chimney, which greatly decreases the melting temperature of the liquid. This second effect is localized in the region where the streamlines are upturned because the diffusion of solute has been ignored. Thus, the effects of heat loss are felt further from the chimney boundary than those of solute-induced changes in the melting temperature. The net result of these two competing effects is a solid fraction that first increases very sharply near the chimney boundary, then decays slowly across the mushy layer, reaching a minimum value at the symmetry line dividing two chimney catchment regions.

Examining figure 5(*a–c*), one sees that the solid-fraction contours near the chimney wall become increasingly vertical as the flow amplitude increases, indicating that the flat-wall approximation works well in this limit. At low amplitudes, however, we find that the approximation is poor, and it gives rise to anomalous behaviour in the limit of the chimney width going to zero. An analysis of the details in the vicinity of the pinch-off point would require different scalings than those presented here; we anticipate that a more refined model will reveal that solutions in this poorly

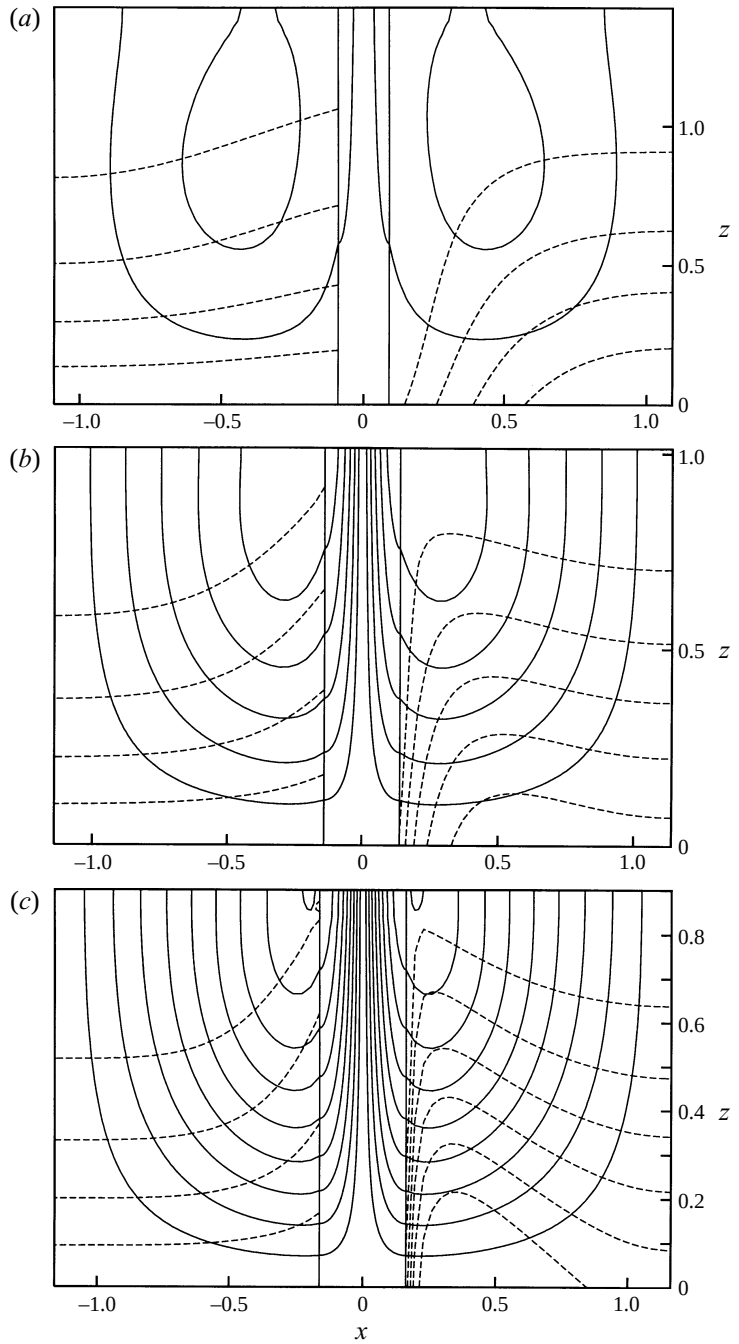

FIGURE 5. Streamlines in both the chimney and mushy regions, along with contours for temperature and solid fraction in the mushy region for (*a*) $Ra = 24$, lower branch, (*b*) $Ra = 24$, upper branch and (*c*) $Ra = 30$, upper branch. In all three cases $\mathscr{C} = 10$, $S = 1$, $\theta_\infty = 0.1$, $Da = 0.001$, $L = 1.0$ and we have used the SOR method with a 30 by 30 mesh. The contour values for the right-hand-side streamlines are $\psi = 0.1$ to $\psi = 1.5$ by 0.2 increments, starting from the outside. The temperature contours (dashed lines) are shown on the left-hand side of the mushy region only, and their values are $\theta = -1.0$ to $\theta = 0$ by 0.2 increments. Solid fraction contours (dashed curves on right-hand side of mushy region) have values in the range $\phi = 0$ to $\phi = 0.15$ by 0.03 increments, starting from the top. Note that not all of these contour values appear in every figure.

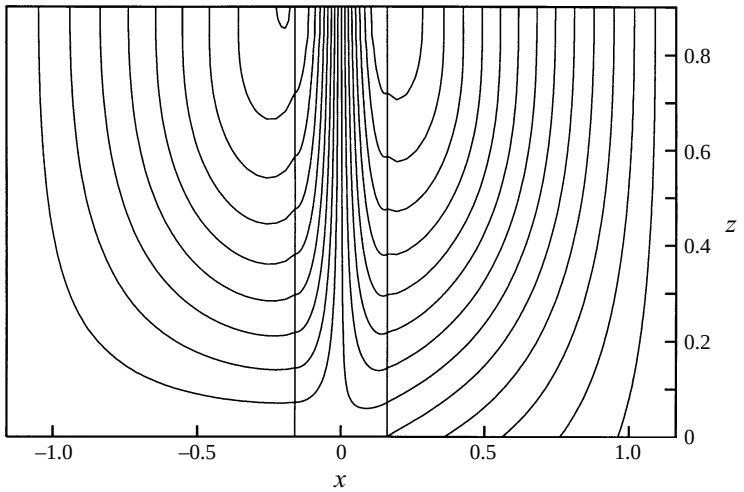

FIGURE 6. The right-hand side of this figure shows the streamlines from figure 5(*c*) redrawn with a streamfunction that is measured relative to a reference frame that moves with the interface. In this frame of reference streamlines do correspond to particle paths, and the vertical velocity is equal to the pulling speed at the lower boundary. For comparison, the streamlines as viewed from the laboratory frame are shown on the left-hand side of the figure.

modelled region are composed of states featuring partially formed chimneys which pinch off well before reaching the bottom of the mushy layer. The slope of the contours near the base of the chimney wall supports the arguments put forward in §3 that fully developed chimneys also become narrower and pinch off (D. E. Loper, private communication) near the bottom of the mushy layer when solidification is forced at constant speed.

In interpreting this figure it is important to remember that the velocity and streamfunction are measured in a frame of reference fixed with respect to the solid phase. This is done in keeping with the traditional notation in the directional solidification literature, but has the disadvantage that the fluid particles do not follow streamlines. In figure 6 we have redrawn figure 5(*c*) with a streamfunction that is measured relative to a reference frame that moves with the interface. In this figure streamlines do correspond to particle paths, and the vertical velocity is equal to the pulling speed at the lower boundary. This latter reference frame makes it easy to see a qualitative distinction between convection with and without chimneys – chimneys do not form until material escapes from the top of the mushy layer. Convection may still be present when all of the material flowing into the mushy layer exits the mushy layer by becoming frozen into the solid. In the purely conductive case, these streamlines are vertical.

5.2. *Bifurcation structure*

The presence of a subcritical solution branch may be understood in terms of physical mechanisms with the aid of figure 3(*a*). When the Rayleigh number is small, the flow can be shut down entirely by making the chimney sufficiently narrow. Thus, along the lower branch of the curve, the existence of a solution with non-zero flux is dependent on the increased permeability produced by widening the chimney. For a fixed value of the Rayleigh number, one finds that increasing the width of the chimney (and, hence, the strength of the flow) near the lower branch causes the solid fraction to drop as more and more rejected solute is swept upward through the chimney wall, causing

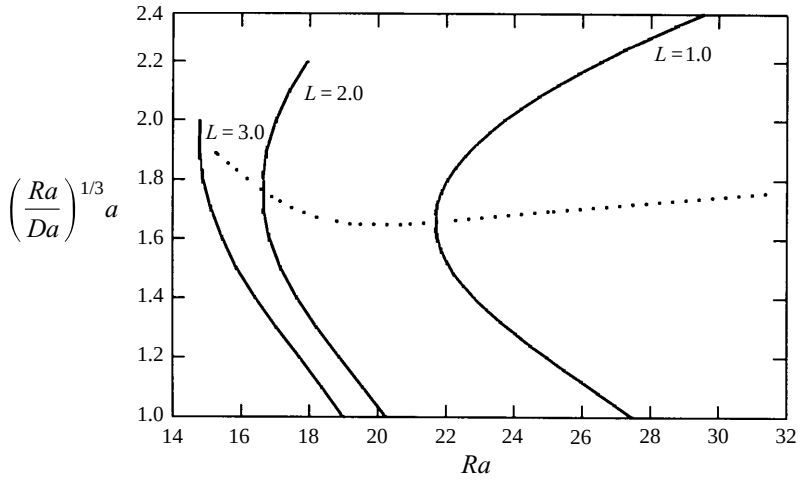

FIGURE 7. The dashed curve shows the location of the turning point as L is varied from 0.5 to 2.7 with the parameters $\mathscr{C}$, θ_∞ and S held fixed at the values used in the previous figures. The three solid curves represent the solution as Ra is varied for L fixed at 1.0, 2.0 and 3.0. The figure demonstrates that the point where the numerical method fails moves closer to the turning point as L is increased.

solid to melt. Thus, the solid fraction on the chimney wall crosses zero as the chimney is widened in the vicinity of the lower branch. Further increases in the chimney width eventually lead to a flattening of the streamlines entering the chimney. When this happens, the rejected solute is swept into the chimney before turning upward, and thus avoids melting solid near the chimney wall. After this point has been reached, further increases in the chimney width result in an increased solid fraction near the chimney wall as the cold liquid passing through the chimney draws heat from the mushy region. This eventually leads to the solid fraction on the chimney wall returning to zero, at which point there is a second, presumably stable, chimney branch. Only the second mechanism continues to work at higher Rayleigh numbers, where strong flows are present even in the absence of chimneys.

In figure 7 we consider the dependence of the system on the chimney spacing L. The dotted curve shows the location of the turning point as L is varied from 0.5 to 2.7 with the parameters $\mathscr{C}$, θ_∞ and S held fixed at the values used in the previous figures. The three solid curves represent the solution as Ra is varied for L fixed at 1.0, 2.0 and 3.0. As the width of the cell grows, one expects to reach a critical width where there is enough buoyant fluid to sustain two cells. If this critical width could be determined at the turning point for the solution curve, one would have the global critical Rayleigh number, i.e. the Rayleigh number below which an arbitrarily large periodic disturbance of any wavelength would decay. However, as seen in figure 7, this point, if it exists, is at a flow amplitude which is beyond our ability to calculate successfully, owing to a numerical instability within the thermal boundary layer.

In experiments, this global critical Rayleigh number is likely to correspond to solutions of such large amplitude that they never occur, so that the chimney spacing is determined instead by the level of noise in the system. For a fixed chimney strength $\mathscr{A}$, we find that increasing the chimney spacing does eventually lead to the formation of a second convection cell. In the case under investigation here, this happens at a value of L which is roughly the same order of magnitude ($L \approx 3$) as half the linear critical wavelength, indicating that the preferred chimney spacing is considerable

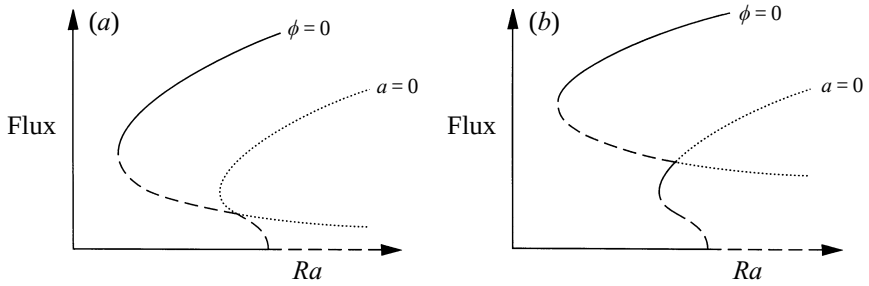

FIGURE 8. Drawing of a conjectured bifurcation diagrams showing flux versus *Ra*. The complete solution curve corresponding to physically relevant equilibrium solutions includes the stable (solid) and unstable (dashed) portions of the diagrams. The remaining (dotted) portions of the diagrams correspond to non-physical solutions having either $a < 0$ or $\phi < 0$. In (*a*) the chimney curve intersects the unstable portion of the non-chimney curve, while in (*b*) the intersection of the chimney and non-chimney curves occurs on the stable portion of the non-chimney curve, indicating that there is a hysteresis loop between solutions with and without chimneys.

smaller than the linear theory would predict. Our choice of $L = 1.0$ for most of the calculations was motivated by experimental results which seem to indicate an $O(1)$ aspect ratio for the portion of a convection half-cell contained within the mushy layer (see figure 1) and by the fact that we could achieve larger amplitude solutions without encountering numerical difficulties. Obtaining a quantitative result for the preferred chimney spacing will require extensive investigation beyond the present study.

Another point of significant interest is the transition from fully nonlinear convective solutions which lack chimneys to solutions with chimneys. This transition occurs when fluid starts to rise through the mushy layer and prevents solidification within the chimney, necessitating a change in the type of boundary condition applied at the point where a plume emerges from the top of the mushy layer (i.e. $T = 0$ is no longer appropriate.) In the model with the flat chimney wall, this transition is deemed to occur when the solid fraction at mid-height on the chimney wall first becomes negative. (Note that the development referred to here occurs as the Rayleigh number is varied, as opposed to a temporal development.)

In figure 8(*a, b*) we draw conjectured bifurcation diagrams for two possible cases. In both cases the volume flux of fluid into the layer from above is plotted as a function of the Rayleigh number for solutions with ($\phi_w = 0, a > 0$) and without ($\phi_w \neq 0, a = 0$) chimneys. The area to the right of the chimney ($\phi = 0$) curve can be understood to correspond to non-physical solutions with negative solid fraction on the chimney wall, with the area to the left of the curve corresponding to non-equilibrium solutions having positive solid fractions on the chimney wall. Similarly, the $a = 0$ curve divides the flux–Rayleigh-number plane into a section with non-physical solutions having negative chimney widths (right-hand side of curve) and a section having positive chimney widths. In the first case (figure 8*a*) the transition to chimneys occurs on the lower, presumably unstable, branch of the non-chimney solutions and in the second case it occurs on the upper, presumable stable, branch. As first noted in the weakly nonlinear analysis of Anderson & Worster (1995), there is an important distinction between these cases: when the intersection occurs on the lower branch of the non-chimney curve (figure 8*a*) there will be no stable convective solutions that do not feature chimneys, while in the second case there may be a small range of Rayleigh numbers where one can find stable convective solutions without chimneys. Our numerical results suggest that both cases can occur.

6. An improved approximation for the shape of mush–liquid interface

As noted previously, the flat-topped mushy layer does not occur in practice. Using the condition that the top of the mushy layer is an isotherm and the boundary condition (3.9) on the chimney wall, we can see that the slope of the mush–liquid interface at the point where it meets the chimney wall should be

$$h_x = -T_x/T_z = -\psi. \tag{6.1}$$

Forcing a flat top onto the system, despite (6.1), leads to a discontinuity in the thermal field. (The adverse effects of this can be seen in figure 5(*c*) if one looks carefully at the isotherms near the top of the chimney.) This discontinuity is readily repaired by constructing a boundary condition which is consistent with (3.14) in the outer mushy region, but reduces to (6.1) in the corner of the mushy region near the chimney opening. An appealing and simple choice for this condition is one that converts (3.14) into an ODE with an appropriate boundary layer structure:

$$\delta h_{xx} - h = -h_0, \tag{6.2}$$

where h_0 is the height that would be determined by (3.14) alone. The solution of this equation compatible with both end conditions is

$$h(x) = h_0 + \frac{\psi_c \delta}{\sinh(L/\delta)} \left(1 - \cosh\left(\frac{L-x}{\delta}\right)\right), \tag{6.3}$$

where ψ_c is the value of the streamfunction in the corner near the chimney. The appropriate boundary layer thickness in the large Rayleigh number limit discussed in §3 is the thermal boundary layer thickness $\delta \sim Ra^{-2/3}$.

This boundary condition is incorporated into the numerical analysis using the domain fixing transformation:

$$\zeta = z/h(x). \tag{6.4}$$

The resulting nonlinearities in the governing equations are dealt with by using data from the previous iteration in our numerical scheme. Figure 9 shows the result of a calculation using (6.3) for the same parameter values used in figure 5(*b*). Here, the small volcano-shaped structure at the chimney exit may be seen explicitly, and there is no discontinuity in the thermal field. Comparing with figure 1, we see that the top of the mushy layer in this figure has a realistic shape.

7. Summary and conclusions

In this paper we have analysed convection in a mushy layer using a model that treats the layer as a porous medium with a solid-fraction-dependent permeability. Zero-solid-fraction chimney regions were analysed using lubrication theory, and, subsequently, a Polhausen approximation. We began our analysis by identifying a distinguished limit which reveals a complicated boundary layer structure for highly permeable mushy layers at large Rayleigh numbers. The boundary-layer equations outside the chimney region were found to offer no essential simplification over the full governing equations. Hence, we adopted numerical techniques in the mushy layer and coupled them to lubrication solutions in the chimney region. In order to facilitate extensive numerical calculations within the mushy region, we used the approximation that both the chimney wall and the top of the mushy layer were flat but free to move in the direction normal to the coordinate axes. As a step toward

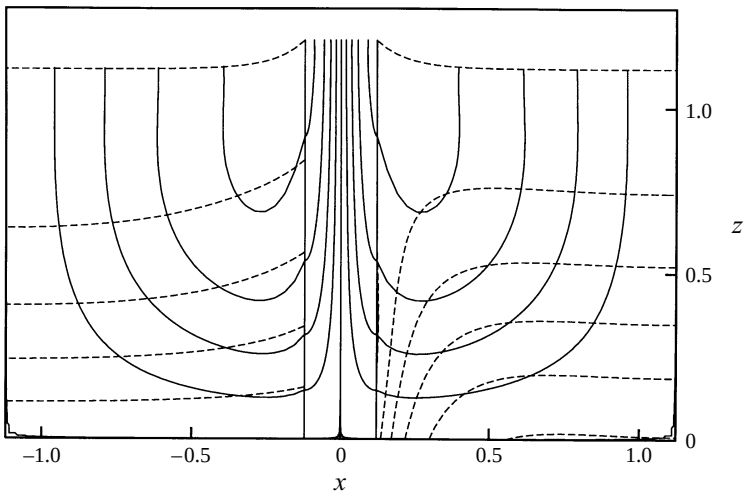

FIGURE 9. A picture analogous to that in figure 5(*b*) but using the approximation (6.3) for the top of the mushy layer.

a more accurate model, we explored the use of an *ad hoc* boundary condition that links together in a consistent way local approximations for the top of the mushy layer.

The numerical solutions reveal the thermal boundary layer predicted by the scaling analysis, even at relatively moderate values of the Rayleigh number. The boundary layer was seen to feature a solid fraction which first increases very rapidly from zero near the chimney, and then decreases as one moves toward the outer region of the mushy layer. Isotherms were seen to slope upward as one moves toward the chimney within this boundary layer, while they were much flatter in the outer region. It is encouraging that, even within the flat-top approximation, the shape of the isotherms echoes the volcano-shaped structures that have been widely observed to form at chimney openings (compare figure 1 and 5*c*).

A key finding of the numerics was that there are two distinct chimney solutions at sufficiently low Rayleigh numbers, presumably corresponding to the stable and unstable portions of a subcritical bifurcation. The unstable portion of this bifurcation appears to connect with convective solutions with no chimney. The transition to chimneys is the result of the qualitative change in the flow pattern when flow begins re-emerging from the top of the mushy layer. It appears that this transition can occur on either the stable or unstable portion of the non-chimney solution. In the former case there can be a hysteresis between strongly nonlinear solutions with and without chimneys.

This work was supported by a grant from the National Aeronautics and Space Administration through the Program on Microgravity Science and Applications and by the NSF-NATO postdoctoral fellowship program. The authors are grateful to J. R. Lister for several helpful discussions, to D. M. Anderson and R. C. Kerr for examining an earlier draft of this manuscript and to D. E. Loper for pointing out that the chimney cannot extend to the bottom of the mushy layer for the case of continuous solidification.

REFERENCES

Amberg, G. & Homsy, G. M. 1993 Nonlinear analysis of buoyant convection in binary solidification with application to channel formation. *J. Fluid Mech.* **252**, 79–98.

Anderson, D. M. & Worster, M. G. 1995 Weakly nonlinear analysis of convection in mushy layers during the solidification of binary alloys. *J. Fluid Mech.* **302**, 307–331.

Bennon, W. D. & Incropera, F. P. 1987 The Evolution of Macrosegregation in Statically Cast Binary Ingots. *Metall. Trans.* B **18**, 611–616.

Chen, C. F. 1995 Experimental study of convection in a mushy layer during directional solidification. *J. Fluid Mech.* **293**, 81–98.

Chen, F., Lu, J. W. & Yang, T. L. 1994 Convective instability in ammonium chloride solution directionally solidified from below. *J. Fluid Mech.* **276**, 163–187.

Copley, S. M., Giamei, A. F., Johnson, S. M. & Hornbecker, M. F. 1970 The origin of freckles in unidirectionally solidified castings. *Metall. Trans.* **1**, 2193–2204.

Eide, L. I. & Martin, S. 1975 The formation of brine drainage features in young sea ice. *J. Glaciology* **14**, 137–154.

Emms, P. W. 1993 Compositional convection and freckle formation in the solidification of binary alloys. PhD thesis, University of Oxford, UK.

Emms, P. W. & Fowler, A. C. 1994 Compositional convection in the solidification of binary alloys. *J. Fluid Mech.* **262**, 111–139.

Fearn, D. R., Loper, D. E. & Roberts, P. H. 1981 Structure of the Earth's inner core. *Nature* **292**, 232–233.

Felicelli S. D., Heinrich, J. C. & Poirier, D. R. 1991 Simulation of freckles during vertical solidification of binary alloys. *Metall. Trans.* B **22**, 847–859.

Fowler, A. C. 1985 The formation of freckles in binary alloys. *IMA J. Appl. Maths* **35**, 159–174.

Hellawell, A., Sarazin, J. R. & Steube, R. S. 1993 Channel convection in partly solidified systems. *Phil. Trans. R. Soc. Lond.* A **345**, 507–544.

Hills, R. N., Loper, D. E. & Roberts, P. H. 1983 A thermodynamically consistent model of a mushy zone. *Q. J. Mech. Appl. Maths* **36**, 505–539.

Mullins, W. W & Sekerka, R. F. 1964 Stability of a planar interface during solidification of a binary alloy. *J. Appl. Phys.* **35**, 444–451.

Neilson, D. G. & Incropera, F. P. 1991 Unidirectional solidification of a binary alloy and the effects of induced fluid motion. *Intl J. Heat Mass Transfer* **34**, 1717–1732.

Neilson, D. G. & Incropera, F. P. 1993 Effect of rotation on fluid motion and channel formation during unidirectional solidification of a binary alloy. *Intl J. Heat Mass Transfer* **36**, 485–505.

Press, W. H., Teukoisky, S. A., Vettering, W. T. & Flannery, B. P. 1992 *Numerical Recipes*. Cambridge University Press.

Roberts, G. O. 1979 Fast viscous Bénard convection. *Geophys. Astrophys. Fluid Dyn.* **12**, 235–272.

Roberts, P. H. & Loper, D. E. 1983 Towards a theory of the structure and evolution of a dendrite layer. *Stellar and Planetary Magnetism* (ed. A. M. Soward), pp. 329–349. Gordon Breach.

Sarazin, J. R. & Hellawell, A. 1988 Channel formation in Pb-Sn, Pb-Sb, and Pb-Sn-Sb alloy ingots and comparison with the system NH_4Cl-H_2O. *Metall. Trans.* **19A**, 1861–1871.

Solomon, T. H. & Hartley, R. R. 1998 Measurements of the temperature field of mushy and liquid regions during solidification of aqueous ammonium chloride. *J. Fluid Mech.* **358**, 87–106.

Tait, S. & Jaupart, C. 1992 Compositional convection in a reactive crystalline mush and melt differentiation. *J. Geophys. Res.* **97**, 6735–6756.

Turcotte, D. L. 1967 A boundary layer theory for cellular convection. *Intl J. Heat Mass Transfer* **10**, 639–674.

Wettlaufer, J. S., Worster, M. G. & Huppert, H. E. 1997 The evolution of sea ice: solute trapping and brine-channel formation. *J. Fluid Mech.* **344**, 291–316.

Worster, M. G. 1991 Natural convection in a mushy layer. *J. Fluid Mech.* **224**, 335–359.

Worster, M.G. 1992*a* The dynamics of mushy layers. In *Interactive Dynamics of Convection and Solidification* (ed. S. H. Davis, H. E. Huppert, U. Müller & M. G. Worster), pp. 113–138. Kluwer.

Worster, M. G. 1992*b* Instabilities of the liquid and mushy regions during solidification of alloys. *J. Fluid Mech.* **237**, 649–669.

Worster, M. G. 1997 Convection in mushy layers. *Ann. Rev. Fluid Mech.* **29**, 91–122.